

# Carbon sequestration in the deep Atlantic enhanced by Saharan dust

Katsiaryna Pabortsava<sup>1\*</sup>, Richard S. Lampitt<sup>1</sup>, Jeff Benson<sup>1</sup>, Karen Casciotti<sup>2</sup>, Christian Crowe<sup>1</sup>, Robert McLachlan<sup>1</sup>, Frédéric A. C. Le Moigne<sup>3</sup>, C. Mark Moore<sup>4</sup>, Corinne Pebody<sup>1</sup>, Paul Provost<sup>1</sup>, Andrew Rees<sup>5</sup>, Gavin Tilstone<sup>5</sup> and E. Malcom S. Woodward<sup>5</sup>

**Enhanced atmospheric input of dust-borne nutrients and minerals to the remote surface ocean can potentially increase carbon uptake and sequestration at depth. Nutrients can enhance primary productivity, and mineral particles act as ballast, increasing sinking rates of particulate organic matter. Here we present a two-year time series of sediment trap observations of particulate organic carbon flux to 3,000 m depth, measured directly in two locations: the dust-rich central North Atlantic gyre and the dust-poor South Atlantic gyre. We find that carbon fluxes are twice as high and a higher proportion of primary production is exported to depth in the dust-rich North Atlantic gyre. Low stable nitrogen isotope ratios suggest that high fluxes result from the stimulation of nitrogen fixation and productivity following the deposition of dust-borne nutrients. Sediment traps in the northern gyre also collected intact colonies of nitrogen-fixing *Trichodesmium* species. Whereas ballast in the southern gyre is predominantly biogenic, dust-derived mineral particles constitute the dominant ballast element during the enhanced carbon fluxes in the northern gyre. We conclude that dust deposition increases carbon sequestration in the North Atlantic gyre through the fertilization of the nitrogen-fixing community in surface waters and mineral ballasting of sinking particles.**

Flux of airborne desert dust into the surface ocean can increase the amount of photosynthetically fixed carbon dioxide (CO<sub>2</sub>) by reducing nutrient limitation of primary production, and thus increase the flux of particulate organic carbon (POC) to the deep ocean<sup>1</sup>. Dense dust-derived lithogenic particles can also increase particle size through aggregation, and enhance sinking velocity and preservation of POC through ballasting, allowing more carbon to penetrate deeper into the ocean's interior<sup>2</sup>. The impact of dust input on downward POC flux can be especially important in the subtropical low-nutrient, low-chlorophyll (oligotrophic) gyres which occupy 60% of the global ocean surface<sup>3</sup>, and thus are probably large sinks for atmospheric CO<sub>2</sub> (ref. 4). Even relatively small changes in downward POC flux in these immense areas would significantly affect the global carbon budget. However, the transport of organic carbon (that is, Biological Carbon Pump) in oligotrophic regions is very poorly understood, and large uncertainties remain over the impact of enhanced dust deposition on the magnitude of POC flux below the depth of winter mixing (sequestration).

We tested the hypothesis that enhanced dust deposition increases POC sequestration in remote low-nutrient, low-chlorophyll provinces by directly measuring downward deep POC flux in the centres of the subtropical North and South Atlantic gyres. The study regions represent permanently stratified systems characterized by restricted nutrient advection, and hence extremely low surface concentrations of macronutrients (nitrate and phosphate) and chlorophyll. Here, picoplankton dominate community structure<sup>5</sup>, while heterotrophic bacteria and cyanobacteria govern ecosystem metabolism, channelling a large proportion of POC into the microbial loop<sup>6</sup>, thus diminishing its export out of the euphotic zone. The subtropical North Atlantic, however, receives large

depositional fluxes of Saharan dust with associated essential nutrients (for example, nitrogen, phosphorus, iron)<sup>1</sup> blocked from the South Atlantic region by the Inter-Tropical Convergence Zone<sup>7</sup>. The Fe-rich surface waters of the northern gyre are favoured by N<sub>2</sub>-fixing microbes (diazotrophs) that generate bioavailable nitrogen for other phytoplankton<sup>8</sup>, thereby allowing for a higher proportion of primary production to be converted into sinking POC than would otherwise occur. Phosphate co-limits the Fe-induced N<sub>2</sub> fixation and production fuelled by atmospheric nitrogen<sup>9,10</sup>. This can exert an important control over the amount of POC ultimately produced from diazotrophic and atmospheric sources, and subsequently available for export. Along with this fertilization effect, increased lithogenic particle concentration following dust input can also facilitate POC flux to depth through additional incorporation of dense dust particles<sup>11</sup>. Biomineral ballasting is otherwise regulated by calcite which is typically found in both gyres<sup>12</sup>. However, the degree to which lithogenic ballasting can drive the increased POC sedimentation would itself be limited by the amount of POC present<sup>13</sup>.

## Field observations in the central Atlantic gyres

We directly captured POC flux in the centres of the oligotrophic gyres of the North Atlantic (NOG; 23° N 41° W) and South Atlantic (SOG; 18° S 25° W) from 2007 to 2010 using sediment traps moored at 3,000 m depth (Fig. 1). During this period, NOG was subjected to, on average, tenfold higher dust deposition compared to SOG (Fig. 2a), as inferred from dust concentration measurements over Barbados<sup>14</sup> for NOG and modelled data<sup>15,16</sup> for SOG (Methods). At both sites, the average surface production rates derived from a Vertically Generalized Production Model (VGPM)<sup>17</sup> were lower

<sup>1</sup>National Oceanography Centre, European Way, Southampton, UK. <sup>2</sup>Stanford University, Department of Environmental Earth System Science, Stanford, California 94305, USA. <sup>3</sup>GEOMAR Helmholtz Centre for Ocean Research, Kiel, Germany. <sup>4</sup>University of Southampton, Waterfront Campus, European Way, Southampton, UK. <sup>5</sup>Plymouth Marine Laboratory, Plymouth, UK. \*e-mail: [katsia@noc.ac.uk](mailto:katsia@noc.ac.uk)

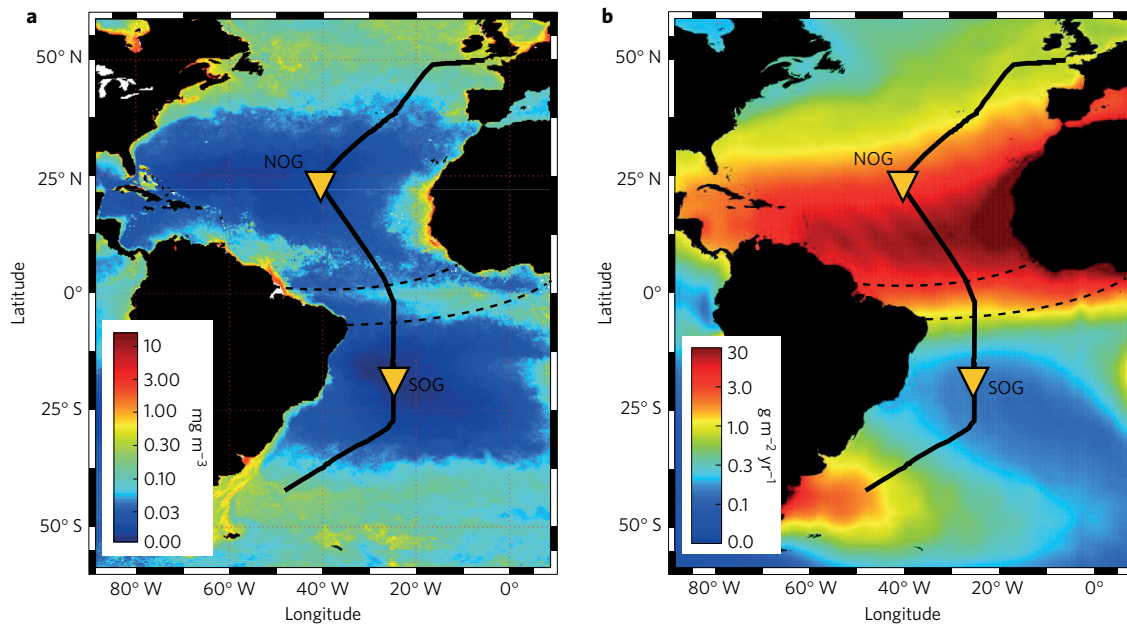


**Figure 1 | Chlorophyll and dust deposition flux in the Atlantic Ocean.** **a**, Annual composite Moderate-Resolution Imaging Spectroradiometer (MODIS) chlorophyll-*a* concentration ( $\text{mg m}^{-3}$ ) in 2009. Oligotrophic gyres are represented by dark blue areas of low chlorophyll concentrations ( $<0.1 \text{ mg m}^{-3}$ ). **b**, Basin-wide annually averaged (1974–2004) modelled dust deposition flux re-plotted from ref. 16. Yellow triangles indicate the locations of the NOG and SOG sediment trap moorings, which are also on the annually repeated Atlantic Meridional Transect (AMT) line ([www.amt-uk.org](http://www.amt-uk.org)). The black solid line shows the AMT-19 cruise track (October–November 2009) passing through the NOG and SOG sites. Dashed lines indicate an approximate north–south boundary of the Inter-Tropical Convergence Zone.

1 than in much of the global ocean<sup>18</sup>, and on average 23% higher at  
 2 NOG than at SOG (Fig. 2b). The observed POC fluxes to the trap  
 3 at NOG ( $0.40\text{--}2.7 \text{ mg C m}^{-2} \text{ d}^{-1}$ ; mean =  $1.06 \text{ mg C m}^{-2} \text{ d}^{-1}$ ) were  
 4 always at least twofold higher than at SOG ( $0.21\text{--}0.95 \text{ mg C m}^{-2} \text{ d}^{-1}$ ;  
 5 mean =  $0.49 \text{ mg C m}^{-2} \text{ d}^{-1}$ ) (Figs 2d and 3). The POC fluxes at NOG  
 6 and SOG were significantly lower than the depth-normalized values  
 7 reported for the oligotrophic sites in the western North Atlantic gyre  
 8 (station OFP (BATS))<sup>19</sup> and subtropical North Pacific gyre (station  
 9 ALOHA)<sup>20</sup>, and hence they are among the lowest in the global  
 10 ocean. From the ratios of POC flux to VGPM primary production  
 11 (both variables were averaged over the trap deployment period) we  
 12 calculate almost double the fraction of surface production reaching  
 13 3,000 m depth at NOG (0.60%) compared to SOG (0.37%). These  
 14 very low values are similar to the records at BATS (0.59%)<sup>19</sup> and  
 15 imply an overall more efficient downward POC transport in the  
 16 dusty northern gyre. Lithogenic flux determined from aluminium  
 17 concentrations in trap material was significantly lower at SOG  
 18 than at NOG (Fig. 2c) and elsewhere in the subtropical North  
 19 Atlantic<sup>19,21</sup>, indicating that the inter-basin differences in dust  
 20 deposition propagated to depth. The NOG data bridge the previous  
 21 observations of deep lithogenic flux in the eastern and western  
 22 parts of the northern gyre<sup>19,21</sup> showing the westward gradient of  
 23 decreasing deep lithogenic fluxes driven by the weakening of the  
 24 Saharan dust transport towards the northwest Atlantic<sup>14</sup>.

25 Although higher at NOG, at both sites POC flux increased  
 26 during late summer–autumn (Fig. 3), a period of warm sea surface  
 27 temperature ( $>25^\circ\text{C}$ ), shallow mixed layer ( $<50 \text{ m}$ ), and low  
 28 surface chlorophyll concentrations ( $<0.04 \text{ mg m}^{-3}$ ) (Supplementary  
 29 Fig. 1). Seasonality of POC flux at our study sites is similar to  
 30 that at ALOHA<sup>20</sup>, but different from BATS, where the highest  
 31 fluxes occur in spring<sup>19</sup>. At NOG, elevated POC flux coincided  
 32 with periods of enhanced dust deposition (Fig. 3a). At the time of  
 33 the weakest exchange between surface nutrient-poor and deeper  
 34 nutrient-rich waters, dust was probably an important source of  
 35 ‘new’ nutrients stimulating biological growth<sup>1</sup>. Dust deposited in  
 36 summer has a much lower nitrogen to phosphorus ratio compared

to that in winter<sup>22</sup>. Hence, some increase in primary production  
 could occur through utilization of solely dust-derived nitrogen and  
 phosphorus by all primary producers, including nitrogen fixers<sup>23</sup>.  
 Dust also supplies excess of iron<sup>23</sup> which could trigger increased  
 diazotrophy in the nitrogen-limited, warm and stable water column  
 at NOG<sup>8–10</sup>. Diazotrophs would then alleviate nitrogen stress and  
 deplete the pool of bioavailable phosphorus<sup>8–10</sup>. Almost threefold  
 increases in  $\text{N}_2$  fixation rates by diazotroph *Trichodesmium* spp.  
 were observed in the region of NOG during summer–autumn  
 (median  $34.9 \mu\text{mol N m}^{-2} \text{ d}^{-1}$ ) compared to winter–spring (median  
 $12.2 \mu\text{mol N m}^{-2} \text{ d}^{-1}$ ) (refs 24–27). This is consistent with higher  
 deposition of dust-derived iron<sup>28</sup> and subsequent enhanced surface  
 concentrations of dissolved iron observed at NOG during summer–  
 autumn<sup>29,30</sup>. Very low concentrations of surface phosphate and  
 higher utilization rates of dissolved organic phosphorus in the  
 summer at NOG provide further evidence for iron-induced  
 enhancement of diazotrophy<sup>8</sup>.

We observe a remarkably high POC flux of up to  
 $2.7 \text{ mg C m}^{-2} \text{ d}^{-1}$  in August–September 2009 at NOG (Fig. 3a). This  
 relatively short POC export pulse, never seen at SOG, accounted  
 for 29% of total POC sequestered at NOG during 2007–2009  
 and greatly exceeded the mean wintertime POC flux at NOG  
 ( $0.88 \pm 0.13 \text{ mg C m}^{-2} \text{ d}^{-1}$ ) and the daily flux at SOG. A notable  
 presence of some intact *Trichodesmium* ‘tufts’ (Figs 3a and 4) within  
 this pulse suggests a potential involvement of these diazotrophs in  
 driving the extreme POC sequestration event at NOG. Similarly  
 short and efficient POC export pulses to  $>2,800 \text{ m}$  depth have  
 been regularly observed at ALOHA following a summertime  
 increase in productivity and biomass of diatom–diazotroph  
 symbiotic phytoplankton<sup>20</sup>.

### Fertilization effect of dust

We measured low stable nitrogen isotope ratios in the trap  
 material ( $\delta^{15}\text{N}_{\text{PN}}$ , in ‰ relative to air) from the dust-rich NOG  
 (range  $0.40\text{--}1.32\text{‰}$ ; mass-weighted mean  $0.77\text{‰}$ ) (Figs 2 and 3a),  
 indicating that isotopically light nitrogen introduced by enhanced

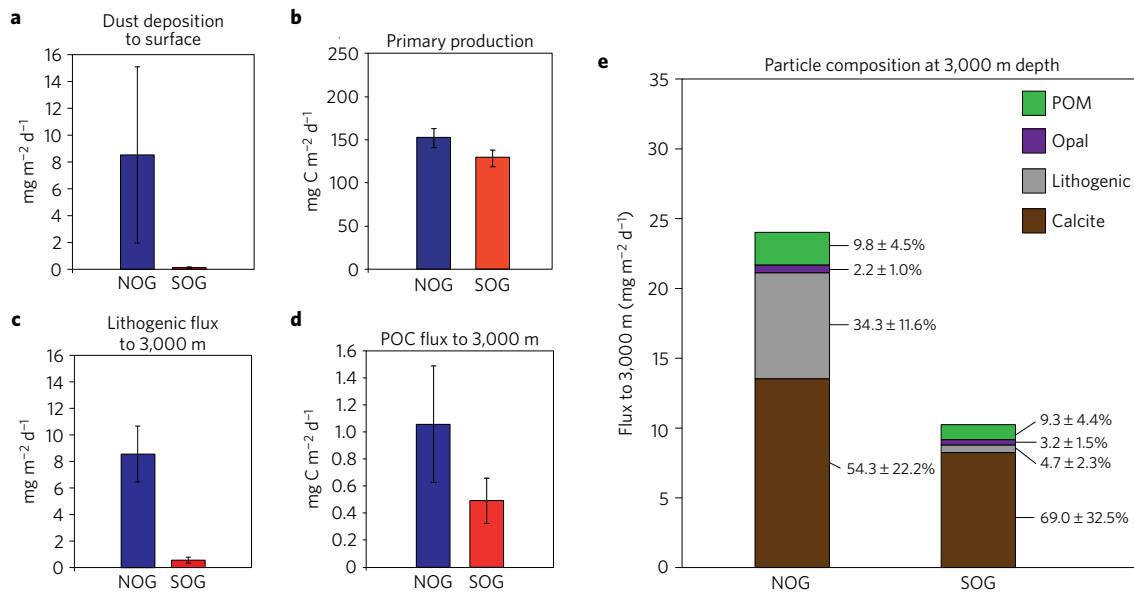


**Figure 2 | Surface ocean and deep particle flux data for the study sites. a–d,** Mean  $\pm$  standard deviation values over the respective trap deployment periods. **a,** Dust deposition flux ( $n=25$  for NOG and  $n=26$  for SOG). **b,** Depth-integrated primary production derived from the chlorophyll-based Vertically Generalized Production Model<sup>17</sup> ( $n=124$  for both sites; Methods). **c,** Lithogenic flux ( $n=40$  for both sites). **d,** POC flux ( $n=40$  for both sites). **e,** Composition of sediment trap material. The height of the stacked bars represents total particle mass flux.

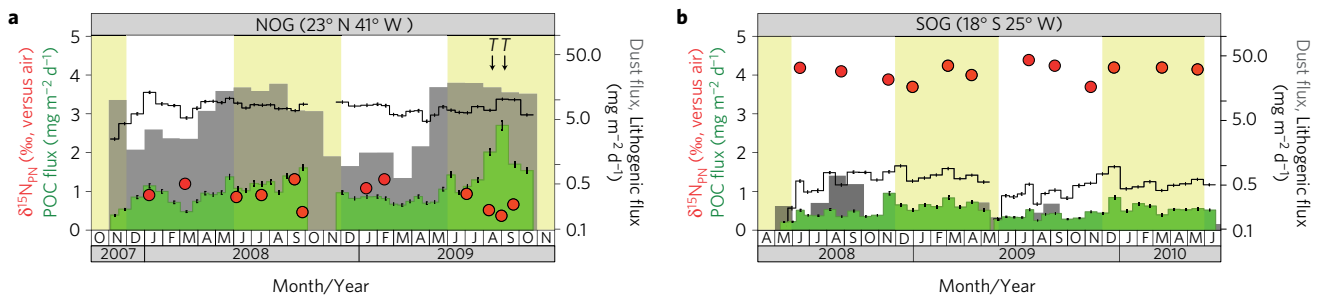


**Figure 3 | Time-series fluxes at NOG (a) and SOG (b).** The dust deposition (monthly values) and aluminium-derived lithogenic fluxes are presented on a logarithmic scale. The uncertainty of the dust flux to the South Atlantic is estimated to be at least a factor of ten (ref. 16). For POC and lithogenic fluxes, the width of each bar corresponds to 14- or 21-day collection intervals. Red circles depict stable nitrogen isotopic composition of particles ( $\delta^{15}N_{PN}$ ) from the selected cups. Arrows and a letter 'T' indicate the cups where *Trichodesmium* spp. 'tufts' were found. Summer–autumn periods are highlighted in yellow.

Q.4

1  $N_2$  fixation and potentially atmospheric deposition<sup>31</sup> significantly  
 2 contributed to sinking particles. Some of this low  $\delta^{15}N$  signal  
 3 might have originated south of NOG ( $10^\circ$ – $16^\circ$  N), before being  
 4 transported to and accumulated at the NOG thermocline as low-  
 5  $\delta^{15}N$  nitrate during northward water mass transit<sup>3,32</sup>. However, a  
 6 strong inverse correlation between  $\delta^{15}N_{PN}$  and POC flux ( $R^2=0.67$ ,  
 7  $p=0.001$ ) with *Trichodesmium* 'tufts' present at the lowest  $\delta^{15}N_{PN}$   
 8 values (Figs 4 and 5) is suggestive of a direct link between elevated  
 9 POC flux at NOG and a local supply of newly fixed nitrogen by  
 10 diazotrophs whose activity was probably stimulated by substantial  
 11 inputs of dust-borne iron. Observations at NOG are qualitatively  
 12 similar to those at ALOHA<sup>20</sup>, where  $\delta^{15}N_{PN}$  minima and diazotroph-  
 13 driven particulate POC flux maxima are closely associated. Dust  
 14 deposition, which is a substantial source of isotopically light  
 15 nitrogen in the region ( $8.5 \mu\text{mol m}^{-2} \text{d}^{-1}$ ; ref. 23) could augment the  
 16 deep POC flux, lowering its  $\delta^{15}N$  signature.  
 17 In contrast to NOG, sinking particles from the dust-poor SOG  
 18 carried significantly higher  $\delta^{15}N_{PN}$  of 3.70‰ to 4.41‰ (mass-  
 19 weighted mean 4.07‰). This is similar to the oceanic average  $\delta^{15}N$   
 20 of deep-water nitrate (4.8‰; ref. 31), and hence this source was  
 21 probably fuelling primary production at SOG.  
 22 The deep  $\delta^{15}N_{PN}$  at NOG and SOG fit a broad range of  $\delta^{15}N$   
 23 values reported for particulate nitrogen in the upper waters of the

Atlantic oligotrophic gyres<sup>33,34</sup> (Supplementary Fig. 2). At both sites,  
 trap material was  $^{15}N$ -enriched compared to the particles suspended  
 in the euphotic zone (top 130 m). While the latter incorporate  
 recycled nitrogen, remineralization-derived fractionation during  
 sinking probably increased  $\delta^{15}N_{PN}$  values<sup>35</sup>. Similar  $\delta^{15}N$  values  
 for trap material and particles from 150–160 m depth point to a  
 potentially important contribution of higher  $\delta^{15}N$  signal formed at  
 the deep chlorophyll maximum to  $\delta^{15}N_{PN}$ . However, fractionation  
 effects associated with incomplete nitrate assimilation within lower  
 regions of the nitracline might also play a role.  
 We estimated the contribution of different nitrogen sources  
 to  $\delta^{15}N_{PN}$  at NOG and SOG using a two-endmember nitrogen  
 mass-balance model<sup>31</sup> (see Methods and references therein). We  
 assumed that the isotope budget of the mixed layer in the  
 permanently oligotrophic gyres incorporates nitrogen supplied by  
 diazotrophs, by vertical diffusion across the nitrate concentration  
 gradient, and from dust (NOG only). We also assumed negligible  
 isotopic fractionation following complete nitrogen assimilation  
 by phytoplankton. The average isotopic signature of diazotrophic  
 biomass ( $-1 \pm 1\text{‰}$ ) was used as the  $N_2$  fixation endmember. The  
 upper thermocline nitrate endmember was represented by  $\delta^{15}N$   
 nitrate averaged over the depth of the nitrate gradient spanning the  
 euphotic layer at NOG ( $2.73 \pm 0.36\text{‰}$ ) and SOG ( $6.22 \pm 0.35\text{‰}$ ).



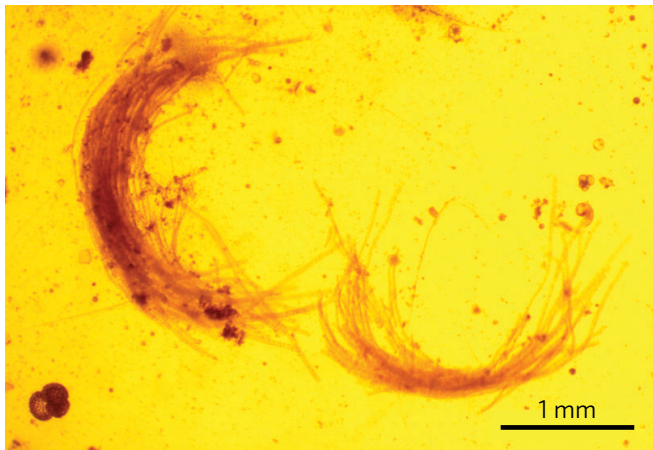


**Figure 4** | *Trichodesmium* spp. 'tufts' from the summer POC flux pulse at NOG. Tufted colonies of *Trichodesmium* spp. cells were identified in the cups collecting in August and September 2009. This is the first record of *Trichodesmium* being exported to bathypelagic depth (>1,500 m).

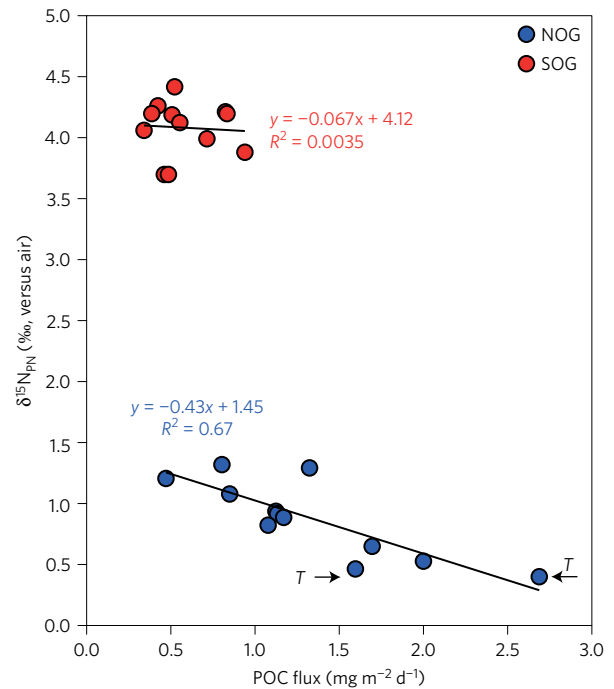


**Figure 5** | POC flux versus isotopic composition of the trap material ( $\delta^{15}\text{N}_{\text{PN}}$ ) from NOG (blue circles) and SOG (red circles). The black line is the best fit line of the linear model. Arrows with letter 'T' mark the cups where *Trichodesmium* tufts were found. The strong inverse relationship between the magnitude of POC flux and  $\delta^{15}\text{N}_{\text{PN}}$  at NOG signifies a potentially important role of local input of isotopically light N from  $\text{N}_2$  fixation (and dust deposition) in enhancing carbon sequestration at this site.

density and allowing them to sink rapidly to depth and avoid remineralization or grazing. This could partly explain the temporal coherence between low  $\delta^{15}\text{N}_{\text{PN}}$  and elevated fluxes of dust, POC and lithogenic material during late summer at NOG (Fig. 3a).

### Ballasting effect of dust

Higher dust input significantly altered the composition of particles at NOG compared to SOG (Fig. 2e). Dust-derived lithogenic material was the second largest contributor ( $34.3 \pm 11.6\%$ ) to the total mass at NOG after calcite, whereas at SOG this value was  $4.7 \pm 2.3\%$ , consistent with the difference in the amount of dust being deposited at each site (Fig. 2a). Although the seasonal signal of elevated dust flux at both sites was largely lost at 3,000 m depth, we still observed elevated lithogenic flux at NOG (>120% of the annual average) in winter 2008 and summer–autumn 2008 and 2009 concurrently with the increased POC flux and following high dust input (Fig. 3a). Assuming that this temporal coherence was not accidental, we investigated the relative involvement of lithogenic and biogenic (opal + calcite) ballast phases in enhanced POC sequestration. Based on the outputs of the mineral-associated POC flux model and multiple linear regression analysis<sup>2,43</sup> (Methods), 41.0% of POC flux at SOG was ballasted by lithogenic material. This, however, might be an overestimation driven by a relatively large carrying coefficient for lithogenic ballast (0.371) which resulted from a nearly 1:1 ratio of POC to lithogenic flux and their strong positive correlation (Spearman's  $p = 0.91$ ). At NOG the percentage of POC ballasted by lithogenic particles increased from 45.7% during low POC flux to 70.1% during high flux in the summer–autumn (Supplementary Table 2). Overall, lithogenic material appears to be a more important ballast for POC in the central northern gyre compared to its western boundary (25% at BATS), where lithogenic fluxes are lower and opal fluxes are ten times higher<sup>19</sup>. We suggest that at NOG elevated

The dust-derived nitrogen endmember was assigned  $\delta^{15}\text{N}$  of  $-3.1\%$ , based on the average isotopic composition of bulk aerosols influenced by Saharan dust. Using these endmember values, we find that local  $\text{N}_2$  fixation could contribute on average  $50.4 \pm 8.4\%$  to the isotopic signal of nitrogen sequestration at NOG, while aerosol nitrogen alone (if all bioavailable) could account for  $32.4 \pm 5.4\%$  (Supplementary Table 1). The contribution of diazotrophs to  $\delta^{15}\text{N}_{\text{PN}}$  at NOG was higher than that at BATS<sup>35,36</sup> and at ALOHA (range 21–48%; refs 20,37), where eddy transfer and lateral advection are important mechanisms of nitrogen supply<sup>37,38</sup>. At SOG, newly fixed nitrogen contributed a smaller, yet considerable portion of  $\delta^{15}\text{N}_{\text{PN}}$  ( $29.7 \pm 3.1\%$ ), possibly owing to the activity of unicellular cyanobacteria, major  $\text{N}_2$  fixers in the South Atlantic<sup>8,27</sup>. We, however, acknowledge a significant uncertainty of these results due to an overall lack of time-resolved  $\delta^{15}\text{N}$  data for the surface nitrate and dust at the trap sites. Moreover, our budgets did not account for a possible origin of particles from a specific trophic level (for example, faecal pellets) and alteration of  $\delta^{15}\text{N}_{\text{PN}}$  due to isotopic fractionation during particle remineralization and transformation in the mesopelagic<sup>35</sup>. However, regardless of these uncertainties, the isotope budgets suggest a large systematic difference in the contribution of newly fixed local nitrogen inputs between the North and South Atlantic gyres which probably contributes to the twofold inter-basin difference in POC sequestration. Our observations thus set an important quantitative constraint on the downward flux of low  $\delta^{15}\text{N}$  material sinking to the subtropical North Atlantic. They provide compelling evidence for the origin of an isotopically light nitrate reservoir in the thermocline of the subtropical North Atlantic, supporting previous observations (for example, ref. 32).

The unique presence of intact *Trichodesmium* colonies in the deep particles at NOG (Fig. 4) indicates that *Trichodesmium* biomass is not always lost in the surface waters as previously assumed<sup>39,40</sup>, but can leave the euphotic zone and contribute to POC export. It is possible that the 'tufts' reached the abyssal depth at NOG in a rapidly sinking (>200  $\text{m d}^{-1}$ ) *Trichodesmium* bloom, collapsed through viral lysis or programmed cell death<sup>40</sup>. Since iron starvation at NOG is unlikely, exhaustion of bioavailable phosphorus<sup>9,10</sup> during the summer might be a major trigger of the bloom collapse. Alternatively, the 'tufts' might represent *Trichodesmium* populations that migrated towards the phosphocline to 'mine' phosphate but were unable to return to the light<sup>41</sup>. Finally, *Trichodesmium* can retain dust particles within their morphologically intricate colonies to accelerate iron dissolution from dust<sup>42</sup>. Trapped dust particles may therefore 'ballast' *Trichodesmium* colonies, increasing their

dust inputs may shift the dominant ballasting phase from biogenic to lithogenic, increasing POC flux to the deep ocean. This is likely achieved through a sudden increase in mineral particle concentration following dust deposition and subsequent stimulation of aggregation of organic matter, including that of diazotrophs, in the surface waters<sup>11</sup>. Moreover, clay particles, constituting >60% of the aerosol dust over the central North Atlantic<sup>44</sup>, are denser (2.79 g cm<sup>-3</sup>) than biomineral calcite (2.65 g cm<sup>-3</sup>) and opal (2.1 g cm<sup>-3</sup>), and thus might increase sinking velocity of POC upon aggregation. Although currently debated in the literature (for example, refs 45,46), lithogenic ballast might also exert an enhanced protective effect on POC compared to calcite. Laboratory experiments<sup>46,47</sup> demonstrated slower degradation rates for clay-ballasted POC relative to calcite-ballasted POC. The existence of such a protective effect of lithogenic material is yet to be shown in the field.

### Mechanism of dust-induced enhancement of carbon sequestration

The ballasting ability of lithogenic particles at NOG appears to be confined to the summer–autumn period (Fig. 3a) when the surface fertilization by dust was potentially the strongest. This tight temporal coupling suggests that the presence of additional fresh organic matter (that is, fertilization effect) might be required to activate effective lithogenic ballasting while lithogenic particles are critical to transport the fertilization effect to the deep ocean. The variability in mineralogy and morphology of dust arriving at NOG from different locations in the Sahara during winter and summer<sup>48</sup> may have also impacted both the fertilization and ballasting properties of dust.

Overall, enhanced POC sequestration in the dust-rich NOG suggests that, in the vast nutrient-limited Atlantic, the strength of the biological carbon pump could be significantly lower without concurrent dust-induced fertilization and ballasting. The observed twofold enhancement of POC sequestration under a tenfold higher dust (iron) input at NOG further points to a potentially important role of phosphate in setting the upper bound for the iron-driven enhancement of POC export<sup>8–10</sup>. However, fertilization could also stimulate the activity of heterotrophic bacteria, increasing remineralization and a corresponding reduction of carbon export<sup>5</sup>.

Under the current climatic trends, the subtropical oligotrophic gyres are predicted to expand over the coming centuries<sup>49</sup>. Multi-decadal observations of dust concentrations over Barbados have already revealed a weakening of dust transport from North Africa to the North Atlantic as a function of increasing sea surface temperature<sup>14</sup>. Predicted changes in wind patterns are expected to continue altering dust deposition into the ocean, and hence input of nutrients and mineral ballast<sup>50</sup>. In parallel, ongoing ocean acidification might affect bioavailability of essential nutrients, including iron<sup>51</sup>. All these perturbations will certainly alter POC sequestration in the oligotrophic gyres, and hence global climate, in the coming centuries. Therefore, our study urges for a better understanding of the present Biological Carbon Pump functioning in the nutrient-limited oceans.

### Methods

Methods, including statements of data availability and any associated accession codes and references, are available in the [online version of this paper](#).

Received 15 September 2016; accepted 20 January 2017; published online XX Month XXXX

### References

- Jickells, T. *et al.* Global iron connections between desert dust, ocean biogeochemistry, and climate. *Science* **308**, 67–71 (2005).
- Klaas, C. & Archer, D. E. Association of sinking organic matter with various types of mineral ballast in the deep sea: implications for the rain ratio. *Glob. Biogeochem. Cycles* **16**, 63–61–63–14 (2002).

- Antoine, D., André, J. M. & Morel, A. Oceanic primary production: 2. Estimation at global scale from satellite (Coastal Zone Color Scanner) chlorophyll. *Glob. Biogeochem. Cycles* **10**, 57–69 (1996).
- Tilstone, G. H. *et al.* Satellite estimates of net community production indicate predominance of net autotrophy in the Atlantic Ocean. *Remote Sens. Environ.* **164**, 254–269 (2015).
- Zubkov, M. V., Sleight, M. A., Tarran, G. A., Burkill, P. H. & Leakey, R. J. Picoplanktonic community structure on an Atlantic transect from 50° N to 50° S. *Deep-Sea Res. I* **45**, 1339–1355 (1998).
- Marañón, E. *et al.* Degree of oligotrophy controls the response of microbial plankton to Saharan dust. *Limnol. Oceanogr.* **55**, 2339–2352 (2010).
- Schlosser, C. *et al.* Seasonal ITCZ migration dynamically controls the location of the (sub) tropical Atlantic biogeochemical divide. *Proc. Natl Acad. Sci. USA* **111**, 1438–1442 (2014).
- Moore, C. M. *et al.* Large-scale distribution of Atlantic nitrogen fixation controlled by iron availability. *Nat. Geosci.* **2**, 867–871 (2009).
- Mather, R. L. *et al.* Phosphorus cycling in the North and South Atlantic Ocean subtropical gyres. *Nat. Geosci.* **1**, 439–443 (2008).
- Mills, M. M., Ridame, C., Davey, M., La Roche, J. & Geider, R. J. Iron and phosphorus co-limit nitrogen fixation in the eastern tropical North Atlantic. *Nature* **429**, 292–294 (2004).
- Lee, C. *et al.* Particulate organic matter and ballast fluxes measured using time-series and settling velocity sediment traps in the northwestern Mediterranean Sea. *Deep-Sea Res. II* **56**, 1420–1436 (2009).
- Poulton, A. J., Adey, T. R., Balch, W. M. & Holligan, P. M. Relating coccolithophore calcification rates to phytoplankton community dynamics: regional differences and implications for carbon export. *Deep-Sea Res. II* **54**, 538–557 (2007).
- Passow, U. & De La Rocha, C. L. Accumulation of mineral ballast on organic aggregates. *Glob. Biogeochem. Cycles* **20** (2006).
- Prospero, J. M., Collard, F.-X., Molinié, J. & Jeannot, A. Characterizing the annual cycle of African dust transport to the Caribbean Basin and South America and its impact on the environment and air quality. *Glob. Biogeochem. Cycles* **28**, 757–773 (2014).
- Luo, C., Mahowald, N. M. & Del Corral, J. Sensitivity study of meteorological parameters on mineral aerosol mobilization, transport, and distribution. *J. Geophys. Res.* **108** (2003).
- Mahowald, N., Luo, C., Del Corral, J. & Zender, C. S. Interannual variability in atmospheric mineral aerosols from a 22-year model simulation and observational data. *J. Geophys. Res.* **108** (2003).
- Behrenfeld, M. J. & Falkowski, P. G. Photosynthetic rates derived from satellite-based chlorophyll concentration. *Limnol. Oceanogr.* **42**, 1–20 (1997).
- Emerson, S. Annual net community production and the biological carbon flux in the ocean. *Glob. Biogeochem. Cycles* **28**, 14–28 (2014).
- Conte, M. H., Ralph, N. & Ross, E. H. Seasonal and interannual variability in deep ocean particle fluxes at the Oceanic Flux Program (OFP)/Bermuda Atlantic Time Series (BATS) site in the western Sargasso Sea near Bermuda. *Deep-Sea Res. II* **48**, 1471–1505 (2001).
- Karl, D. M., Church, M. J., Dore, J. E., Letelier, R. M. & Mahaffey, C. Predictable and efficient carbon sequestration in the North Pacific Ocean supported by symbiotic nitrogen fixation. *Proc. Natl Acad. Sci. USA* **109**, 1842–1849 (2012).
- Bory, A. *et al.* Downward particle fluxes within different productivity regimes off the Mauritanian upwelling zone (EUMELI program). *Deep-Sea Res. I* **48**, 2251–2282 (2001).
- Zamora, L. M., Prospero, J. M., Hansell, D. A. & Trapp, J. M. Atmospheric P deposition to the subtropical North Atlantic: sources, properties, and relationship to N deposition. *J. Geophys. Res.* **118**, 1546–1562 (2013).
- Baker, A. *et al.* Dry and wet deposition of nutrients from the tropical Atlantic atmosphere: links to primary productivity and nitrogen fixation. *Deep-Sea Res. I* **54**, 1704–1720 (2007).
- Rees, A. *Rates of Nitrogen Fixation in Surface Waters by Stable-Isotope Mass Spectrometry during the AMT Programme Cruise AMT20 (JC053)* (British Oceanographic Data Centre - Natural Environment Research Council, 2015); <http://dx.doi.org/10.5285/215a1e9b-428b-52f5-e053-6c86abc06d17>
- Snow, J. T. *et al.* Environmental controls on the biogeography of diazotrophy and *Trichodesmium* in the Atlantic Ocean. *Glob. Biogeochem. Cycles* **29**, 865–884 (2015).
- Painter, S. C., Patey, M. D., Forryan, A. & Torres-Valdes, S. Evaluating the balance between vertical diffusive nitrate supply and nitrogen fixation with reference to nitrate uptake in the eastern subtropical North Atlantic Ocean. *J. Geophys. Res.* **118**, 5732–5749 (2013).
- Luo, Y.-W. *et al.* Database of diazotrophs in global ocean: abundance, biomass and nitrogen fixation rates. *Earth Syst. Sci. Data* **4**, 47–73 (2012).
- Baker, A. R., Adams, C., Bell, T. G., Jickells, T. D. & Ganzeveld, L. Estimation of atmospheric nutrient inputs to the Atlantic Ocean from 50° N to 50° S based on large-scale field sampling: Iron and other dust-associated elements. *Glob. Biogeochem. Cycles* **27**, 755–767 (2013).

29. Ussher, S. J. *et al.* Impact of atmospheric deposition on the contrasting iron biogeochemistry of the North and South Atlantic Ocean. *Glob. Biogeochem. Cycles* **27**, 1096–1107 (2013).
30. Conway, T. M. & John, S. G. Quantification of dissolved iron sources to the North Atlantic Ocean. *Nature* **511**, 212–215 (2014).
31. Montoya, J. P. *Stable Isotopes in Ecology and Environmental Science* (eds Michener, R. & Lajtha, K.) Second edn, 176–201 (Blackwell Publishing Ltd., 2007).
32. Knapp, A. N., DiFiore, P. J., Deutsch, C., Sigman, D. M. & Lipschultz, F. Nitrate isotopic composition between Bermuda and Puerto Rico: implications for N<sub>2</sub> fixation in the Atlantic Ocean. *Glob. Biogeochem. Cycles* **22** (2008).
33. Fernández, A., Marañón, E. & Bode, A. Large-scale meridional and zonal variability in the nitrogen isotopic composition of plankton in the Atlantic Ocean. *J. Plankton Res.* **36**, 1060–1073 (2014).
34. Reynolds, S. E. *et al.* How widespread and important is N<sub>2</sub> fixation in the North Atlantic Ocean? *Glob. Biogeochem. Cycles* **21** (2007).
35. Altabet, M. A. Variations in nitrogen isotopic composition between sinking and suspended particles: implications for nitrogen cycling and particle transformation in the open ocean. *Deep Sea Res.* **35**, 535–554 (1988).
36. Knapp, A. N., Sigman, D. M. & Lipschultz, F. N isotopic composition of dissolved organic nitrogen and nitrate at the Bermuda Atlantic Time-series Study site. *Glob. Biogeochem. Cycles* **19** (2005).
37. Dore, J. E., Brum, J. R., Tupas, L. M. & Karl, D. M. Seasonal and interannual variability in sources of nitrogen supporting export in the oligotrophic subtropical North Pacific Ocean. *Limnol. Oceanogr.* **47**, 1595–1607 (2002).
38. Lipschultz, F., Bates, N. R., Carlson, C. A. & Hansell, D. A. New production in the Sargasso Sea: history and current status. *Glob. Biogeochem. Cycles* **16**, 1-1-1-17 (2002).
39. Thompson, A. W. & Zehr, J. P. Cellular interactions: lessons from the nitrogen-fixing cyanobacteria. *J. Phycol.* **49**, 1024–1035 (2013).
40. Mulholland, M. The fate of nitrogen fixed by diazotrophs in the ocean. *Biogeochemistry* **4**, 37–51 (2007).
41. Villareal, T. & Carpenter, E. Buoyancy regulation and the potential for vertical migration in the oceanic cyanobacterium *Trichodesmium*. *Microb. Ecol.* **45**, 1–10 (2003).
42. Rubin, M., Berman-Frank, I. & Shaked, Y. Dust- and mineral-iron utilization by the marine dinitrogen-fixer *Trichodesmium*. *Nat. Geosci.* **4**, 529–534 (2011).
43. Honda, M. C. & Watanabe, S. Importance of biogenic opal as ballast of particulate organic carbon (POC) transport and existence of mineral ballast-associated and residual POC in the Western Pacific Subarctic Gyre. *Geophys. Res. Lett.* **37** (2010).
44. Glaccum, R. A. & Prospero, J. M. Saharan aerosols over the tropical North Atlantic—Mineralogy. *Mar. Geol.* **37**, 295–321 (1980).
45. Iversen, M. H. & Robert, M. L. Ballasting effects of smectite on aggregate formation and export from a natural plankton community. *Mar. Chem.* **175**, 18–27 (2015).
46. Le Moigne, F. A., Gallinari, M., Laurenceau, E. & De La Rocha, C. Enhanced rates of particulate organic matter remineralization by microzooplankton are diminished by added ballast minerals. *Biogeochemistry* **10**, 5755–5765 (2013).
47. Arnarson, T. S. & Keil, R. G. Influence of organic-mineral aggregates on microbial degradation of the dinoflagellate *Scrippsiella trochoidea*. *Geochim. Cosmochim. Acta* **69**, 2111–2117 (2005).
48. Schepanski, K., Tegen, I. & Macke, A. Saharan dust transport and deposition towards the tropical northern Atlantic. *Atmos. Chem. Phys.* **9**, 1173–1189 (2009).
49. Polovina, J. J., Howell, E. A. & Abecassis, M. Ocean's least productive waters are expanding. *Geophys. Res. Lett.* **35** (2008).
50. Jickells, T. & Moore, C. M. The importance of atmospheric deposition for ocean productivity. *Annu. Rev. Ecol. Syst.* **46**, 481–501 (2015).
51. Sunda, W. G. Iron and the carbon pump. *Science* **327**, 654–655 (2010).

## Acknowledgements

We thank the captains and crew of the RRS *Discovery*, RRS *James Clark Ross* and RRS *James Cook* during cruises D324, D334, JCR186, JCR215 and JC05 for deploying and recovering of the McLane sediment traps. We are grateful to M. Cooper, C. Marsay, P. Martin, A. Moje, P. Statham and M. Stinchcombe for their assistance with laboratory work and advice on analytical and sample-handling issues. We thank J. Prospero for providing the Barbados dust concentration data, and N. Mahowald for modelled dust deposition flux data. We thank the British Oceanographic Data Centre and NASA Ocean Colour, and Ocean Productivity website for providing ancillary data. We thank A. Poulton and R. Sanders for participation in results discussion and feedback on this manuscript. This work is a part of doctoral dissertation of K.P. funded by National Oceanography Centre, Southampton and the University of Southampton. This study also contributes to the international IMBER project and was supported by the UK Natural Environment Research Council National Capability funding to Plymouth Marine Laboratory and the National Oceanography Centre, Southampton. This is contribution number 291 of the AMT programme.

## Author contributions

K.P. and R.S.L. designed and conducted the research; K.P. analysed the data and wrote the manuscript together with R.S.L.; J.B., C.C., R.M., P.P. and C.P. coordinated sediment trap operations; F.A.C.L.M. and C.M.M. contributed to the interpretation of the results; K.C., A.R., G.T. and E.M.S.W. provided the ancillary biogeochemical data.

## Additional information

Supplementary information is available in the online version of the paper. Reprints and permissions information is available online at [www.nature.com/reprints](http://www.nature.com/reprints). Correspondence and requests for materials should be addressed to K.P.

## Competing financial interests

The authors declare no competing financial interests.



## Methods

**Particle collection and processing.** Sinking particles were collected using 21-cup time-series Parflux Mark 78H–21 sediment traps (McLane Research Laboratories, USA) deployed on a bottom-tethered mooring at a depth of 3,000 m in a water depth of >4,200 m. At NOG, the traps were deployed from 4 November 2007 to 5 October 2008 and from 23 November 2008 to 25 October 2010, collecting particles over a total of 672 days. At SOG, the traps operated from 11 May 2008 to 20 May 2009 and from 24 May 2009 to 20 June 2010, collecting particles over a total of 766 days. Each trap cup collected for 14 or 21 days. Sample preservative consisted of a solution of sodium chloride (5 g l<sup>-1</sup>), di-sodium tetra-borate (0.25 g l<sup>-1</sup>), and formalin (5% vol/vol) made up with deep seawater. Upon recovery, pH was measured and found to be between 8.0 and 8.3. One ml of concentrated formalin solution was then added to the cups to supplement the existing formalin. Sample processing was carried out under dust- and metal-free conditions in a laminar flow cabinet using plastic- or glass-ware only. Prior to all analyses, zooplankton ‘swimmers’ were identified under a stereo-microscope (Meiji Techno, Japan) fitted with a photo-camera (Canon EOS-1000, Japan) and handpicked using polytetrafluoroethylene (PTFE)-coated tweezers (Dumont, Switzerland) and a plastic pipette (Fisher Scientific). The preservative/particle mixture in each cup was then split into eight sub-samples using a custom-built rotary polyvinyl chloride (PVC) splitter. Individual sub-samples from each cup were filtered, dried at 40 °C and analysed for particulate organic carbon, opal, calcite, and trace metals, including aluminium. Selected sub-samples were also analysed for stable nitrogen isotope composition.

**Chemical analyses of the trap material.** Particulate organic carbon (POC) was measured in tin capsules (HEKAtech GmbH) after removing carbonate by *in situ* acidification<sup>52</sup> with concentrated hydrochloric acid and using a high-temperature combustion technique on a CHN analyser (HEKAtech GmbH EURO EA CHNS-O Elemental Analyser) with an analytical precision of <0.1%. The median filter-blank contribution to POC signal was 2.7%. The calculated limit of detection (LoD; based on three times the standard deviations of the filter blanks) was 8.26 µg (*n* = 20). Particulate Organic Matter (POM) was calculated as 2.2 × POC (ref. 2). Splits for calcite were prepared by leaching in 0.4 mol l<sup>-1</sup> nitric acid with the calcium content measured by inductively coupled plasma optical emission spectrometry<sup>53</sup> (Perkin-Elmer Optima 4300DV ICP-OES; analytical precision of <1%). Procedural blanks consisting of unused polycarbonate membranes treated with nitric acid contributed <1% to the Ca signal. The LoD of the blank-corrected Ca measurements was wavelength-dependent, ranging from 0.012 to 0.015 µg (*n* = 10). Calcite mass flux was calculated by multiplying the calcium-derived flux of particulate inorganic carbon by a factor of 8.3. Samples for opal were digested in 0.2 mol l<sup>-1</sup> sodium hydroxide, neutralized with 0.1 mol l<sup>-1</sup> hydrochloric acid, and analysed as dissolved silicate on a SEAL QuAA Tro auto-analyser<sup>53,54</sup>. The detection limit of the instrument was 0.3 µg. The median contribution of procedural blanks was 3.1%. The LoD of the filter-blank-corrected samples was run-dependent, ranging from 1.19 to 11.5 µg (*n* = 9). Opal was calculated to be 2.4 × biogenic silica flux, assuming 10% water content<sup>53,54</sup>. Labile and refractory fractions of aluminium in trap material were determined<sup>55</sup>. The labile fraction was extracted with 25% (vol/vol) acetic acid at room temperature, and then the more refractory fraction was fully digested in a mixture of concentrated nitric and hydrofluoric acids at 150 °C. The residues of both fractions were redissolved in 0.5 mol l<sup>-1</sup> nitric acid and analysed by inductively coupled plasma-mass spectrometry (Thermo Fisher Scientific Element 2 XR HR-ICPMS). The LoD of blank-corrected aluminium measurements was 0.12 ng g<sup>-1</sup> (*n* = 10); the concentrations in acid mix and blank filters were 0.764 ± 0.8 ng g<sup>-1</sup>; (*n* = 10) and 0.843 ± 0.917 ng g<sup>-1</sup> (*n* = 8), respectively. The accuracy of the measurements was established using a range of Certified Reference Materials, including HISS-1, NIST-1648a and NIST-1573a. The recoveries in these reference materials were 97.3–104.1% for aluminium. Total trace metal concentration was determined by adding leach and digest metal fractions. Total aluminium mass flux was used to calculate lithogenic mass flux based on an aluminium content of 7.1% in Saharan dust<sup>56</sup> and 7.7% in Patagonian dust<sup>57</sup> for NOG and SOG samples, respectively. The stable nitrogen isotopic composition of the sinking particulate nitrogen pool ( $\delta^{15}\text{N}_{\text{PN}}$ ) was determined from the <sup>14</sup>N/<sup>15</sup>N mass ratio measured using a Micro Cube elemental analyser (Elementar Analysensysteme GmbH) interfaced to a PDZ Europa 20-20 isotope ratio mass spectrometer (Sercon Ltd.). The accuracy of the measurements was established using a set of laboratory standards calibrated against NIST Standard Reference Materials (IAEA-N1, IAEA-N2, IAEA-N3, USGS-40, and USGS-41). The analytical precision of the  $\delta^{15}\text{N}_{\text{PN}}$  measurements was <0.1‰, while the difference between duplicates ranged between 3.1 and 11% (*n* = 4). Measurements were performed at the UC Davies Stable Isotope Facility, USA.

**Dust deposition flux.** Direct and time-resolved measurements of dust deposition at NOG and SOG are not available. At SOG we obtained monthly estimates of dust deposition using an atmospheric model<sup>15,16</sup>, which utilizes reanalysis data (a combination of model and observations) to drive a dust chemical transport model, and was compared to long-term measurements of aerosol concentration. Dust

deposition flux was modelled in four bins with the size distribution range of 0.1–0.5, 0.5–1.0, 1.0–2.5 and 2.5–10 µm. Dust deposition velocities were calculated within the model as a function of meteorological conditions, and resulted in averages of 0.01, 0.029, 0.115 and 0.674 cm s<sup>-1</sup> over our region. The modelled dust deposition fluxes were averaged for a 3° × 3° area centred at the SOG location. The uncertainty of the model output for the South Atlantic Ocean is hypothesized to be at least a factor of ten due to scarcity and uncertainties in observational data and uncertainties in model source, transport and deposition processes<sup>16</sup>. Dust deposition flux at NOG was inferred from time-series dust concentrations measured over Barbados, which is heavily influenced by air-masses from Sahara and Sahel deserts<sup>14</sup>. The details of dust sampling and processing are described in ref. 14. Dust deposition flux was calculated by multiplying dust concentrations by a range of deposition velocities (0.01–1.2 cm s<sup>-1</sup>) characteristic of relatively fine mineral dust aerosols of <5 µm in size typically arriving to the remote open ocean<sup>58</sup>. The resulting average dust deposition flux at NOG ranged from 0.085 to 10.2 mg m<sup>-2</sup> s<sup>-1</sup>. Assuming a deposition velocity of 1 cm s<sup>-1</sup>, the dust deposition flux is similar in magnitude to the deep lithogenic flux at NOG. Thus, we considered this deposition velocity to be the most appropriate for calculations of daily dust deposition flux at NOG.

**Upper ocean hydrography.** Eight-day composite sea surface temperature (SST) data were recorded by the Moderate-Resolution Imaging Spectroradiometer (MODIS) sensor of NASA’s Aqua satellite at 9 km resolution and averaged for a 3° × 3° box centred at each trap location. The annual cycle of mixed layer depth at the trap sites was derived from the ARGO-based climatology<sup>59</sup> averaged for a 3° × 3° area over the trap sites. The base of the mixed layer was defined as the depth at which the density was 0.03 kg m<sup>-3</sup> less than that at 10 m.

**Ancillary biogeochemical data sets** were provided by the British Oceanographic Data Centre (BODC) and include vertical profiles of chlorophyll (archived data under accession numbers SOC050136 and SOC110235), nitrate concentrations (refs 60,61 and archived data set under accession number MIT130172), isotopic composition of total nitrate (refs 62–64), nitrogen fixation rates (refs 24–26), <sup>14</sup>C-based primary production rates (ref. 65 and archived data with accession numbers PP-PML090162, PP-PML110236 and PP-PML120146).

**Primary production.** Depth-integrated daily rates of primary production for the relevant time period were estimated from the chlorophyll-based eight-day resolved Vertically Generalized Production Model (VGPM)<sup>17</sup> and averaged for the 3° × 3° area centred at the trap sites. The VGPM data were downloaded from the Ocean Productivity website (<http://www.science.oregonstate.edu/ocean.productivity>). Within relevant time periods, the VGPM-based productivity rates at NOG (160 ± 14 mg C m<sup>-2</sup> d<sup>-1</sup>) and SOG (139 ± 18 mg C m<sup>-2</sup> d<sup>-1</sup>) were comparable to the values measured directly at the trap sites in October–November 2008–2011 (240 ± 96 mg C m<sup>-2</sup> d<sup>-1</sup> at NOG and 204 ± 84 mg C m<sup>-2</sup> d<sup>-1</sup> at SOG; see ancillary biogeochemical data sets above).

**Surface chlorophyll-*a* concentration.** Eight-day composite surface chlorophyll-*a* data were recorded by MODIS Aqua at 9 km resolution and averaged for a 3° × 3° box centred at each trap location. MODIS Aqua calculates near-surface chlorophyll concentrations from a model of ocean colour using an empirical relationship.

**Contribution of newly fixed nitrogen to the stable nitrogen isotope signal in trap material.** The  $\delta^{15}\text{N}$  of the trap material reflects both the autotrophic particle formation and the subsequent heterotrophic transformations. In the latter, the diagenetic fractionation can potentially alter  $\delta^{15}\text{N}$  of the bulk nitrogen export and sequestration. No significant relationship was observed between C/N ratios and  $\delta^{15}\text{N}$  of nitrogen export at NOG ( $r^2 = 0.02$ , *n* = 12), while at SOG this relationship was positive, but weak and insignificant ( $r^2 = 0.25$ , *n* = 12). This suggests that the observed variations in  $\delta^{15}\text{N}$  of the trap material were determined predominantly during algal production, with no significant influence from detrital material and/or non-phytoplankton organisms<sup>66</sup>. At both sites, isotopic fractionation following nitrogen assimilation is expected to be negligible due to constant nitrogen limitation in the surface waters<sup>31</sup>. Therefore,  $\delta^{15}\text{N}$  of the produced organic matter should reflect the composition of dominating nitrogen sources to the euphotic zone—namely, upward diffusive flux of deep-water nitrate and N<sub>2</sub> fixation, both having distinct isotopic signals. In addition, in the northern gyre, atmospheric dust deposition can significantly contribute to the total pool of new nitrogen<sup>23,67</sup>. Using equation (1) we describe the isotopic composition of nitrogen export as mixing between diffused nitrogen from the upper thermocline and nitrogen from external sources, represented by either diazotrophy or atmospheric deposition at NOG, and diazotrophy only at SOG:

$$\delta^{15}\text{N}_{\text{PN}} = (f_1 \times \delta^{15}\text{N}_{\text{N}_1}) + (f_2 \times \delta^{15}\text{N}_{\text{N}_2}) \quad (1)$$

where  $f_1$  and  $f_2$  and  $\delta^{15}\text{N}$  denote fractions and isotopic signatures of dominant nitrogen sources. We estimate the percentage contribution of these sources from a

single choice of their respective endmember  $\delta^{15}\text{N}$  values:  $+2.73\text{‰}$  (NOG) and  $+6.22\text{‰}$  (SOG) for nitrate diffusing from the shallow thermocline across the concentration gradient;  $-1.0\text{‰}$  for  $\text{N}_2$  fixation (both sites),  $-3.1\text{‰}$  for bulk aerosol input (NOG only). Due to sensitivity of the two-endmember mixing model to the values of the chosen endmembers, we performed sensitivity analyses to account for uncertainty of the changing  $\delta^{15}\text{N}$  endmembers on the fraction of  $\delta^{15}\text{N}_{\text{PN}}$  (in %) originating from this source at each site, similar to isotopic assessment in ref. 30. The choices of  $\delta^{15}\text{N}$  endmembers for each nitrogen source and those used in the sensitivity tests are described in the section below, and the results are summarized in Supplementary Table 1.

**Sensitivity analyses and  $\delta^{15}\text{N}$  endmember choice.** *Nitrate endmember.* The choice of nitrate  $\delta^{15}\text{N}$  endmember was based on the biogeochemical data (nitrate  $\delta^{15}\text{N}$ , nitrate and chlorophyll concentrations, PAR) obtained at the NOG and SOG sites during AMT cruises in May–June 2005 and October 2005, and US-GEOTRACES cruise GA03 in December 2011 (see ancillary biogeochemical data sets above).

At the permanently oligotrophic NOG and SOG sites, winter mixing is weak, and thermocline nitrate is supplied into the euphotic zone largely by turbulence-driven upward diffusion<sup>68</sup>. The magnitude of diffusive nitrate flux is governed by nitrate concentration gradients as the changes in turbulent diffusivity are relatively small<sup>68</sup>. At both sites, nitrate concentrations remain at nanomolar levels ( $<0.01 \mu\text{mol l}^{-1}$ ) throughout the top 130–150 m and increase below, signifying the position of the nitracline (defined by a nitrate concentration of  $0.1 \mu\text{mol l}^{-1}$ ; for example, ref. 26). The largest nitrate flux with a characteristic  $\delta^{15}\text{N}$  signature is therefore expected at the depth of the maximum nitrate concentration gradient, typically found at depths near the base of the euphotic zone (0.1% surface PAR; includes the deep chlorophyll maximum).

Referring to vertical profiles of nitrate and chlorophyll concentrations, we calculate concentration-weighted average nitrate  $\delta^{15}\text{N}$  (ref. 33) from the top of the nitracline, where nitrate concentrations begin to consistently increase, to the base of the euphotic zone. At NOG this yields nitrate  $\delta^{15}\text{N}$  of  $+2.73 \pm 0.36\text{‰}$  ( $n=5$ ) for the depth range 137–191 m. In our isotopic budgets this value represents an isotopic signal of nitrogen pool influenced by  $\text{N}_2$  fixation and atmospheric deposition, and sustained over time in the shallow thermocline. This is achieved through both the internal cycle of low- $\delta^{15}\text{N}$  nitrate assimilation and subsequent remineralization and accumulation of low- $\delta^{15}\text{N}$  nitrate imported during the northward water mass transit<sup>8,32</sup>. This nitrogen pool has not yet been homogenized with the large global ocean nitrate reservoir ( $\sim 4.8\text{‰}$ ) or  $^{15}\text{N}$ -enriched through denitrification<sup>31,32</sup>. At SOG the most relevant depth range for measured nitrate  $\delta^{15}\text{N}$  spanned 226–230 m, substantially deeper than the base of the euphotic zone. The corresponding mean  $\delta^{15}\text{N}$  of  $+6.22 \pm 0.35\text{‰}$  may thus overestimate the value for the shallower waters, where preferential remineralization of  $^{14}\text{N}$  may introduce a  $^{15}\text{N}$ -depleted signal to the nitrogen pool<sup>31</sup>.

For the primary sensitivity test (Supplementary Table 1) we used the minimal nitrate  $\delta^{15}\text{N}$  observed in the upper thermocline at NOG ( $+0.96\text{‰}$  at 137 m depth) to estimate the least contribution of local  $\text{N}_2$  fixation to  $\delta^{15}\text{N}_{\text{PN}}$ . We also tested nitrate  $\delta^{15}\text{N}$  averaged from the top of nitracline down to the  $26.8 \text{ kg m}^{-3}$  isopycnal surface, which marks the main thermocline depth at the study sites<sup>8,69</sup>. The corresponding value at NOG was  $+3.53 \pm 0.40\text{‰}$  ( $n=13$ ) for the 136–421 m depth range; the SOG value was  $+6.35 \pm 0.32\text{‰}$  ( $n=3$ ) for the 226–306 m depth range. Finally, we included the oceanic global mean  $\delta^{15}\text{N}$  ( $+4.8\text{‰}$ ; ref. 31) to compare our isotope budgets with published data.

**Nitrogen fixation endmember.** We chose the mean  $\delta^{15}\text{N}$  for diazotrophic biomass ( $-1 \pm 1\text{‰}$ ) to represent the  $\text{N}_2$  fixation endmember at both sites<sup>31,70,71</sup>. Assuming the mean nitrate  $\delta^{15}\text{N}$  signal in the shallow thermocline, the range of the isotopic signal for diazotrophic nitrogen ( $-2$ – $0\text{‰}$ ) generates average contributions of 39.8–68.5% and 26.1–34.4% to  $\delta^{15}\text{N}_{\text{PN}}$  at NOG and SOG, respectively (Supplementary Table 1).

**Atmospheric deposition endmember.** Atmospheric fluxes supply approximately  $\sim 9.9 \times 10^9 \text{ mol N yr}^{-1}$  to the central North Atlantic gyre and  $5.8 \times 10^9 \text{ mol N yr}^{-1}$  to the South Atlantic gyre<sup>72</sup>. Although these values are notably smaller than regional estimates of new nitrogen inputs from diazotrophy ( $20 \times 10^{11} \text{ mol N yr}^{-1}$ ; ref. 73), recent studies<sup>23,32,74</sup> suggest that deposition fluxes can significantly lower the  $\delta^{15}\text{N}$  of the nitrogen pool. The published data on  $\delta^{15}\text{N}$  in atmospheric fluxes in the open Atlantic Ocean is extremely scarce. Previous studies<sup>23,74–77</sup> report a wide range of  $\delta^{15}\text{N}$  in bulk aerosol and rainfall samples ( $-6.8\text{‰}$  to  $+1.7\text{‰}$ ). Given that dry deposition dominates atmospheric input at NOG, a value close to an average isotopic signal of bulk aerosols seems the most appropriate to represent the dust endmember at NOG. We thus choose  $\delta^{15}\text{N}$  of  $-3.1\text{‰}$ , based on the mean  $\delta^{15}\text{N}$  values measured in the Sahara-influenced aerosol samples collected in the subtropical North Atlantic<sup>23,75</sup> and Crete<sup>77</sup>. For the sensitivity test, we varied  $\delta^{15}\text{N}$  of atmospheric N across the full range, also including annual ( $-4.5\text{‰}$ ) and seasonal cold ( $-6.8\text{‰}$ ; October–March) and warm ( $-1.9\text{‰}$ ; April–September) averages measured in the Bermuda rainfall<sup>74–76</sup> (Supplementary Table 1). We find that with the nitrate  $\delta^{15}\text{N}$  of  $2.73\text{‰}$ , aerosol nitrogen can account for a sizable fraction of

$\delta^{15}\text{N}$  of nitrogen export at NOG (21.7–176%). Therefore, with nitrogen input equal or greater to magnitude of  $\text{N}_2$  fixation, dust deposition can have a similar or greater effect on the isotopic budget of trap material from NOG. Hence, future studies should include the measurements of both magnitude and  $\delta^{15}\text{N}$  of dust deposition and  $\text{N}_2$  fixation to avoid under- or overestimation of the importance of each source.

**Assessment of ballast effect of lithogenic flux.** We examined the relationship between POC and (bio)mineral at NOG and SOG using POC flux model by ref. 2. The model divides the POC flux into fractions ballasted by biomineral (opal + calcite;  $\text{POC}_{\text{bio}}$ ) and lithogenic ( $\text{POC}_{\text{lit}}$ ) particles, and freely sinking POC ( $\text{POC}_{\text{free}}$ ). We use multiple linear regression to fit the particle flux data into equation (2) and determine correlation coefficients  $a$ ,  $b$  and  $c$  (hereafter, carrying coefficients) for each fraction, following the approach in refs 2,43,78.

$$\text{POC flux} = a \times \text{POC}_{\text{bio}} + b \times \text{POC}_{\text{lit}} + c \times \text{POC}_{\text{free}} \quad (2)$$

Carrying coefficients reflect only the size of the ballast-normalized fraction of the POC flux, but not their absolute magnitudes, and are used to calculate the relative fraction (in %) of POC associated with each ballast type<sup>43,78</sup>. We further assume that the  $\text{POC}_{\text{free}}$  fraction is negligible at 3,000 m depth, and force multiple linear regression to pass through zero<sup>2</sup>. The strong temporal variability of dust deposition limits the relevance of the annual-scale approach for estimating the role of lithogenic ballast to POC flux. Hence, we first assess the effect of lithogenic ballast based on different POC sequestration scenarios: namely, scenario (1) elevated POC flux ( $\geq 120\%$  of annual mean) at NOG, scenario (2) POC flux at NOG outside scenario (1), and scenario (3) POC flux at SOG. Our approach differs from that applied previously by refs 2,43,78 in which carrying coefficients for both calcite and opal were determined. This is due to strong collinearity observed between calcite and opal in all POC-based groups, violating the independence assumption of multiple linear regression, as further determined by ridge regression analysis. The resulting carrying coefficients and calculated proportion of ballast-associated POC flux in each surveyed group are summarized in Supplementary Table 2. The carrying coefficients for lithogenic material compared well with the global and the north Atlantic means (0.052, and 0.058, respectively)<sup>2</sup> during low POC flux, but exceeded these values during high fluxes and overall at SOG. We acknowledge that the relatively large carrying coefficient for lithogenic ballast in the SOG group compared to the NOG groups and other time series might be an overestimation introduced by a nearly 1:1 ratio between POC and lithogenic fluxes and their strong positive correlation (Spearman's  $\rho=0.91$ ). As a result, the proportion of POC flux ballasted by lithogenic material appears to be comparable between SOG and scenario (2) at NOG, despite the significant difference in their lithogenic fluxes (Supplementary Table 2).

We evaluated the sensitivity of these results by performing multiple linear regression on the NOG flux data set separated according to the high and low lithogenic fluxes. Lithogenic particles did not constitute the main ballasting phase for POC during periods of high and low lithogenic fluxes (Supplementary Table 2), and were not associated with biomineral fluxes. This suggests that the presence of POC generated during fertilization is crucial for the effective lithogenic ballasting to occur.

**Data availability.** The data analysed during this study are available from the corresponding author upon request. The supporting data for this study are available from the repository of the British Oceanographic Data Centre upon request.

## References

- Hedges, J. I. & Stern, J. H. Carbon and nitrogen determinations of carbonate-containing solids. *Limnol. Oceanogr.* **29**, 657–663 (1984).
- Salter, I. *et al.* Estimating carbon, silica and diatom export from a naturally fertilised phytoplankton bloom in the Southern Ocean using PELAGRA: a novel drifting sediment trap. *Deep-Sea Res. II* **54**, 2233–2259 (2007).
- Mortlock, R. A. & Froelich, P. N. A simple method for the rapid determination of biogenic opal in pelagic marine sediments. *Deep-Sea Res.* **36**, 1415–1426 (1989).
- Plauquette, H., Fones, G. R., Statham, P. J. & Morris, P. J. Origin of iron and aluminium in large particles ( $>53 \mu\text{m}$ ) in the Crozet region, Southern Ocean. *Mar. Chem.* **115**, 31–42 (2009).
- Guiou, C., Loÿe-Pilot, M. D., Ridame, C. & Thomas, C. Chemical characterization of the Saharan dust end-member: some biogeochemical implications for the western Mediterranean Sea. *J. Geophys. Res.* **107**, ACH 5-1-ACH 5-11 (2002).
- Gaiero, D. M., Probst, J.-L., Depetris, P. J., Bidart, S. M. & Leleyter, L. Iron and other transition metals in Patagonian riverborne and windborne materials: geochemical control and transport to the southern South Atlantic Ocean. *Geochim. Cosmochim. Acta* **67**, 3603–3623 (2003).
- Torres-Padrón, M. *et al.* Variability of dust inputs to the CANIGO zone. *Deep-Sea Res.* **49**, 3455–3464 (2002).



- 1 59. Hosoda, S., Ohira, T., Sato, K. & Suga, T. Improved description of global  
2 mixed-layer depth using Argo profiling floats. *J. Oceanogr.* **66**, 773–787 (2010). 32
- 3 60. Harris, C. & Rees, A. *AMT19 (JC039) Micro-Molar Nutrient Measurements from*  
4 *CTD Bottle Samples* (British Oceanographic Data Centre - Natural  
5 Environment Research Council, 2016);  
6 <http://dx.doi.org/10.5285/42974c1c-ea2d-57a5-e053-6c86abc09d06> 33
- 7 61. Harris, C. & Woodward, E. M. S. *AMT20 (JC053) Micro-Molar Nutrient*  
8 *Measurements from CTD Bottle Samples* (British Oceanographic Data Centre -  
9 Natural Environment Research Council, 2014);  
10 <http://dx.doi.org/10.5285/f3c482e3-245e-36a5-e044-000b5de50f38> 34
- 11 62. Casciotti, K., McIlvin, M. R., Forbes, M. S. & Sigman, D. *Nitrate Isotopes of*  
12 *Nitrate in the GEOTRACES North Atlantic Zonal Transect—Laboratory Casciotti*  
13 (British Oceanographic Data Centre - Natural Environment Research Council,  
14 2016); <http://dx.doi.org/10.5285/2317515c-05c1-6d14-e053-6c86abc0690e> 35
- 15 63. Casciotti, K. *Nitrogen and Oxygen Isotope Measurements of Nitrate from CTD*  
16 *Bottles during Cruise AMT16 (D294)* (British Oceanographic Data Centre -  
17 Natural Environment Research Council, 2015);  
18 <http://dx.doi.org/10.5285/1d4233e0-58e4-637e-e053-6c86abc0ad64> 36
- 19 64. Weigand, A., Marconi, D., Sigman, D. & Casciotti, K. *Nitrate Isotopes of Nitrate*  
20 *in the US GEOTRACES North Atlantic Zonal Transect—Laboratory Sigman*  
21 (British Oceanographic Data Centre - Natural Environment Research Council,  
22 2016); <http://dx.doi.org/10.5285/2317515c-05c0-6d14-e053-6c86abc0690e> 37
- 23 65. Widdicombe, C., Tilstone, G. & Rees, A. *AMT19 (JC039) Primary Production*  
24 *(Size-fractionated) Incubations Using <sup>14</sup>C Uptake from CTD Bottle Samples*  
25 (British Oceanographic Data Centre - Natural Environment Research Council,  
26 2015); <http://dx.doi.org/10.5285/1fecc3c-a422-5d7d-e053-6c86abc0435d> 38
- 27 66. Waser, N. A. D. *et al.* Geographic variations in the nitrogen isotope  
28 composition of surface particulate nitrogen and new production across the  
29 North Atlantic Ocean. *Deep-Sea Res. I* **47**, 1207–1226 (2000). 39
- 30 67. Baker, A., Kelly, S., Biswas, K., Witt, M. & Jickells, T. Atmospheric deposition of  
31 nutrients to the Atlantic Ocean. *Geophys. Res. Lett.* **30** (2003). 40
68. Lewis, M. R., Harrison, W. G., Oakey, N. S., Herbert, D. & Platt, T. Vertical  
nitrate fluxes in the oligotrophic ocean. *Science* **234**, 870–872 (1986). 41
69. Marconi, D. *et al.* Nitrate isotope distributions on the US GEOTRACES North  
Atlantic cross-basin section: signals of polar nitrate sources and low latitude  
nitrogen cycling. *Mar. Chem.* **177**, 143–156 (2015). 42
70. Carpenter, E. J., Harvey, H. R., Fry, B. & Capone, D. G. Biogeochemical tracers  
of the marine cyanobacterium *Trichodesmium*. *Deep-Sea Res. I* **44**,  
27–38 (1997). 43
71. Mahaffey, C., Williams, R. G., Wolff, G. A. & Anderson, W. T. Physical supply  
of nitrogen to phytoplankton in the Atlantic Ocean. *Glob. Biogeochem. Cycles*  
**18** (2004). 44
72. Baker, A. R., Lesworth, T., Adams, C., Jickells, T. D. & Ganzeveld, L. Estimation  
of atmospheric nutrient inputs to the Atlantic Ocean from 50° N to 50° S based  
on large-scale field sampling: fixed nitrogen and dry deposition of phosphorus.  
*Glob. Biogeochem. Cycles* **24**, GB3006 (2010). 45
73. Gruber, N. & Sarmiento, J. L. Global patterns of marine nitrogen fixation and  
denitrification. *Glob. Biogeochem. Cycles* **11**, 235–266 (1997). 46
74. Knapp, A. N., Hastings, M. G., Sigman, D. M., Lipschultz, F. & Galloway, J. N.  
The flux and isotopic composition of reduced and total nitrogen in Bermuda  
rain. *Mar. Chem.* **120**, 83–89 (2010). 47
75. Gobel, A. R., Altieri, K. E., Peters, A. J., Hastings, M. G. & Sigman, D. M.  
Insights into anthropogenic nitrogen deposition to the North Atlantic  
investigated using the isotopic composition of aerosol and rainwater nitrate.  
*Geophys. Res. Lett.* **40**, 5977–5982 (2013). 48
76. Hastings, M. G., Sigman, D. M. & Lipschultz, F. Isotopic evidence for source  
changes of nitrate in rain at Bermuda. *J. Geophys. Res.* **108** (2003). 49
77. Mara, P. *et al.* Isotopic composition of nitrate in wet and dry atmospheric  
deposition on Crete in the eastern Mediterranean Sea. *Glob. Biogeochem. Cycles*  
**23** (2009). 50
78. Le Moigne, F. A. *et al.* On the proportion of ballast versus non-ballast  
associated carbon export in the surface ocean. *Geophys. Res. Lett.* **39** (2012). 51
- 52  
53  
54  
55  
56  
57  
58  
59  
60  
61  
62

## Queries for NPG paper ngeo2899

Page 1

---

*Query 1:*

As per instruction from NPG, the word 'unique' has been deleted here.

*Query 2:*

Please note that reference numbers are formatted according to style in the text, so that any reference numbers following a symbol or acronym are given as 'ref. XX' on the line, whereas all other reference numbers are given as superscripts.

*Query 3:*

Please provide postcode for affiliations 1 and 3–5.

Page 3

---

*Query 4:*

Please provide title (to be in bold) that does not refer to the figure parts themselves for figure 3.

Page 5

---

*Query 5:*

According to style, section headings should not exceed one line in length; please provide a shorter heading that will fit in one line.

*Query 6:*

Please provide page range/article id for refs 13, 15, 16, 32, 34, 36, 43, 49, 67, 71 and 76–78.

Page 6

---

*Query 7:*

F.A.C.L. changed to F.A.C.L.M. in the Author Contribution section, to match the name listed on the first page. Please check.

Page 8

---

*Query 8:*

As per instruction from NPG, the word 'reasonable' has been deleted here.